Energy

WSe$_2$ Thin Film Solar Cells

E. McVay, A. Zubair, M. Hempel, T. Palacios

Our group is interested in exploring the ultimate limits of microsystem scaling and functionality. The amount of energy available to the system is one of the key constraints, and solar cells based on transition metal dichalcogenides (TMDs) could be a key component of future highly-integrated microsystems.

Single atomic layer TMDs have been explored extensively for ultrathin optoelectronic applications due to their direct bandgap and strong light-matter interactions. However, optoelectronic applications of multi-layer TMD thin-films have not been as extensively studied despite their strong absorption characteristics and wide absorption frequency. Nevertheless, published work has shown that a p-n junction made with chemically doped multilayer MoS$_2$ can achieve an efficiency of 2.8%, and a vertical Schottky junction WSe$_2$ solar cell can achieve efficiencies as high as 6.7%. Most intriguingly, it has been shown that with careful design, a 15nm WSe$_2$ solar cell can absorb 90% of 633nm incident light, demonstrating that TMDs can push the limit of thin film photovoltaics.

In this work, we study the electronic transport and photovoltaic characteristics of multilayer (~100 nm) WSe^2 devices that can later be integrated as the energy harvester in a micro-scale sensing system. We have demonstrated a Schottky junction WSe$_2$ solar cell using dissimilar metal contacts. The proof-of-concept dual-metal device showed an open-circuit voltage of ~ 0.2 V, short circuit current density ~ 4 mA/cm^2 and power conversion efficiency ~ 2% under white light illumination with input power of 300 W/m^2. This study is extended to explore methods to better optimize the WSe$_2$ based solar cell using experimental and modeling techniques. We are currently developing hole and electron transport layers to improve the device efficiency.
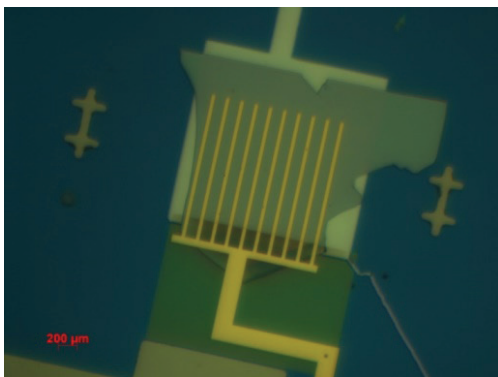
▲ Figure 1: Optical image of a Pt/WSe$_2$/Au solar cell.
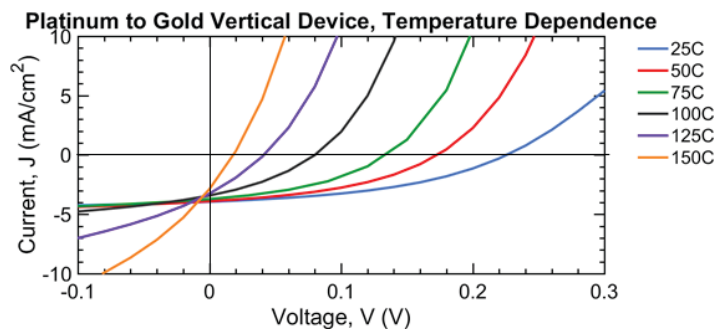
▲ Figure 2: IV-temperature characteristics that demonstrate thermionic emission dominated current and open circuit voltage.

FURTHER READING:

- D. Jariwala, "Near-unity Absorption in van der Waals Semiconductors for Ultrathin Optoelectronics," *Nano Letts.,* vol. 16, no. 9, pp. 5482-5487, 2016.
- S. Wi, "Photovoltaic Response in Pristine WSe$_2$ Layers Modulated by Metal-induced Surface-Charge-Transfer Doping," *Appl. Phys. Letts.,* vol. 107, pp. 062102, 2015.
- S. Wi, "Enhancement of Photovoltaic Response in Multilayer MoS$_2$ Induced by Plasma Doping," *ACS Nano,* vol. 8, no. 5, pp. 5270–5281, 2014.

Critical Design Parameters for Omnidirectional 2-D Filled Photonic Crystal Selective Emitter for Thermophotovoltaics

R. Sakakibara, V. Stelmakh, W. R. Chan, M. Ghebrebrhan, J. D. Joannopoulos, M. Soljačić, I. Čelanović
Sponsorship: ARO, U.S. Department of Energy

Thermophotovoltaic (TPV) systems are promising as small-scale, portable generators to power sensors, small robotic platforms, and portable computational and communication equipment. In TPV systems, an emitter at high-temperature emits radiation that is then converted to electricity by a low bandgap photovoltaic cell. One approach to improve the efficiency is to use hafnia-filled two-dimensional (2-D) tantalum (Ta) photonic crystals (PhCs). These emitters enable efficient spectral tailoring of thermal radiation for a wide range of incidence angles. However, fabricating these PhCs is difficult. We use focused ion beam (FIB) imaging and simulations to investigate the effects of fabrication imperfections on the emittance of a fabricated hafnia-filled PhC and to identify design parameters critical to the overall PhC performance. We demonstrate that, more so than uniform cavity filling, the PhC performance relies on the precise cavity period and radius values and thickness of the top hafnia layer.
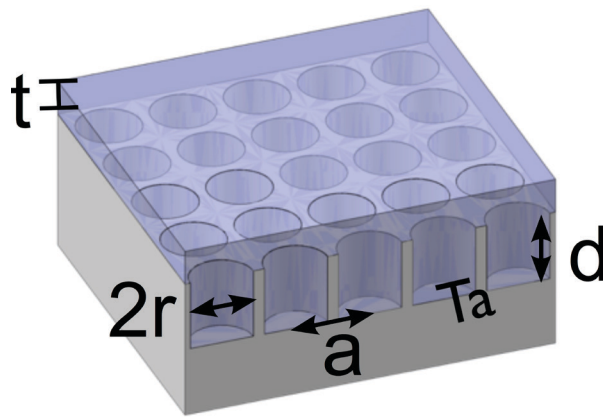
▲ Figure 1: Schematic of a filled photonic crystal (PhC). The geometric parameters are cavity period a, cavity radius r, cavity depth d, and hafnia thickness t. The substrate is tantalum.
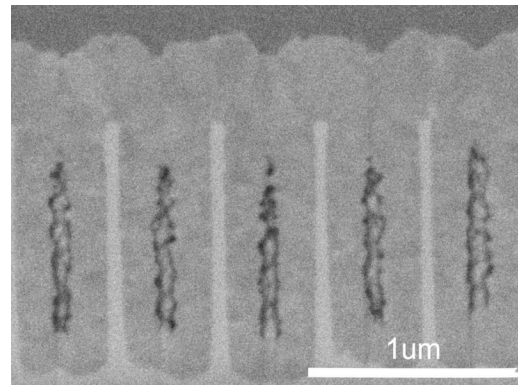
▲ Figure 2: Focused ion beam (FIB) image of the fabricated filled PhC cross section clearly shows incomplete cavity filling and a thick layer of hafnia above the cavity.

FURTHER READING

- W. R. Chan, V. Stelmakh, M. Ghebrebrhan, M. Soljačić, J. D. Joannopoulos, and I. Čelanović, "Enabling Efficient Heat-to-Electricity Generation at the Mesoscale," *Energy Environ. Sci.,* vol. 10, pp. 1367-1371, 2017.
- V. Stelmakh, W. R. Chan, M. Ghebrebrhan, M. Soljačić, J. D. Joannopoulos, and I. Čelanović, "Fabrication of an Omnidirectional 2-D Photonic Crystal Emitter for Thermophotovoltaics," *J. Phys.: Conf. Series,* vol. 773, pp. 012037, 2016.
- Y. X. Yeng, J. Chou, V. Rinnerbauer, Y. Shen, S. G. Kim, J. D. Joannopoulos, M. Soljačić, and I. Čelanović, "Global Optimization of Omnidirectional Wavelength Selective Emitters/Absorbers Based on Dielectric-filled Anti-reflection Coated Two-dimensional Metallic Photonic Crystals," *Opt. Express,* vol. 22, pp. 21711–21718, 2014.

# Low-power Management IC for Vibrational Energy Harvesting Applications

U. Radhakrishna, P. Riehl, N. Desai, P. Nadeau, Y. Yang, A. Shin, D. Ward, J. H. Lang, A. P. Chandrakasan
Sponsorship: Analog Devices, Inc.

Vibration-based machine health monitoring provides an efficient real-time method for tracking the health of industrial motors, thereby achieving predictive maintenance and avoiding machine downtime. Vibration sensors are attached to the vibrating motors, and periodically transmit data indicative of machine health. To power such monitors, we demonstrate a vibration-based energy harvesting system whose schematic is shown in Figure 1. It extracts power from 50Hz industrial motors and comprises a co-designed MEMS-based transducer and associated low-power management circuit.

The MEMS-based energy harvester shown in Figure 1 can generate about 1 mW output power under matched load at resonance. However, its high quality-factor results in significant reduction in output power and voltage at off-resonance conditions. The system is made resilient to manufacturing variations which cause a mismatch between the harvester's natural resonance and the motor frequency by using the interface power electronics. A Meissner oscillator circuit shown in Figure 2 is used to achieve battery-less cold-start from low harvester-voltages at off-resonance. A regular operation circuit is designed to operate once the cold-start circuit generates above-1V output voltage (V_{out}). This circuit employs an H-bridge to interface the harvester whose FETs are switched based on current-feedback. The load-storage element is toggled between the two ports of the harvester to synthesize the desired load-current at any frequency. The circuit thus accomplishes conjugate-impedance matching for efficient power extraction from the harvester. Further, it can tune the harvester's source reactance to electrically shift its resonance to achieve increased bandwidth of operation.

The IC implemented in the Taiwan Semiconductor Manufacturing Company (TSMC) 180nm process (shown in Figure 1) is co-designed with the harvester achieves cold-start from 150mV-peak AC-voltage from the harvester at 5% off-resonance (10x state-of-the-art). The H-bridge circuit is able to deliver 800 μW to the load at 71% efficiency at resonance as shown in Figure 2. It is also able to perform frequency tuning to account for manufacturing tolerances (A first low-power IC demonstration for this application).
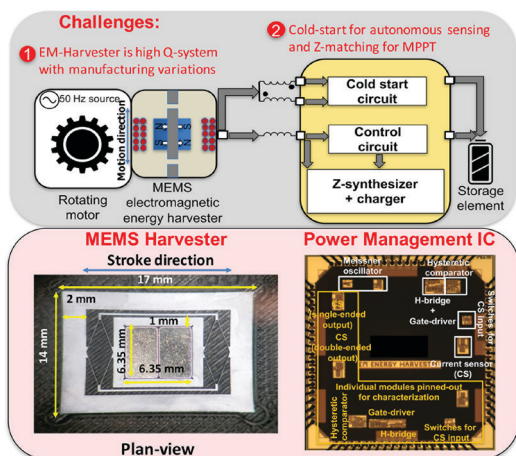
▲ Figure 1: Full system architecture of machine health monitoring system that includes MEMS-based electro-magnetic transducer and interface low-power management integrated circuit implemented in TSMC-180 nm process.
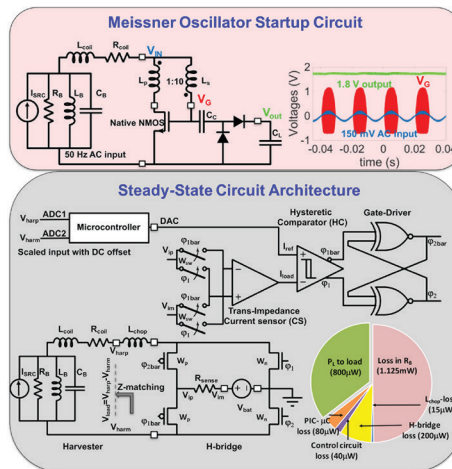
▲ Figure 2: Battery-less cold-startup circuit that starts from V_{IN}=150-200 mV AC-voltage from the harvester to generate V_{INT}=1.1-1.8 V. The regular operation circuit uses an H-bridge circuit to accomplish both impedance matching and frequency tuning.

FURTHER READING

- U. Radhakrishna, P. Riehl, N. Desai, P. Nadeau, Y. Yang, A. Shin, J. H. Lang, and A. P. Chandrakasan, "A Low-power Integrated Power Converter for an Electromagnetic Vibration Energy Harvester with 150 mV-AC Cold Startup, Frequency Tuning, and 50 Hz AC-to-DC Conversion," *IEEE Custom Integrated Circuits Conference (CICC)*, 2018.
- A. Shin, U. Radhakrishna, Q. Zhang, L. Gu, P. Riehl, A. P. Chandrakasan, and J. H. Lang, "A MEMS Magnetic-based Vibration Energy Harvester," *International Conference on Micro and Nanotechnology for Power Generation and Energy Conversion Applications*, (Power MEMS), 2017.

Electromagnetic MEMS Harvester for Vibrational Energy Harvesting Applications

Y. Yang, U. Radhakrishna, P. Riehl, N. Desai, P. Nadeau, A. Shin, D. Ward, J. H. Lang, A. P. Chandrakasan
Sponsorship: Analog Devices, Inc.

Powering machine health monitoring sensors with the motions from the machinery allows install-and-forget implementation of the machine health monitoring network. Electromagnetic MEMS based-transducer provides an efficient interface between industrial machines and the rest of the vibration-based energy harvesting system. Implementing the mechanical harvester's spring system on silicon, allows the mechanical system and the circuit to be manufactured through the same process, cutting down on both assembly time and complexity.

The transducer design uses a modified version of the classic 4 bar linkage spring design. The long beams are tapered such that the end connecting to the guide rod is wider than the connecting region to the shuttle, which houses the magnet (see Figure 1). This alleviates the stress experienced at the joints of the beam, which is the typical weak point of the structure. With the tapered beam, the current design achieves a full stroke of 1.6mm and is more robust with regard to handling during the assembly process. The design also offers good modal separation, with the modal frequency of the first undesirable mode several hundred Hz above the desired, horizontal translational mode.

The coils are manually wound using 42 AWG enamel coated copper wires with two coils placed at 150mm above and below the magnet's plane of motion. The coils and the spring system are each fixed in a plastic package. When attached to the source of vibration, the harvester's magnet vibrates in between the coils, inducing an EMF in the coils in accordance with Lenz's Law. The coils are connected in series, and the induced voltages add to produce an output voltage, which is interfaced with custom designed circuitry for energy harvesting. The assembled mechanical harvester can deliver 1mW of output power at resonance with a matched load.
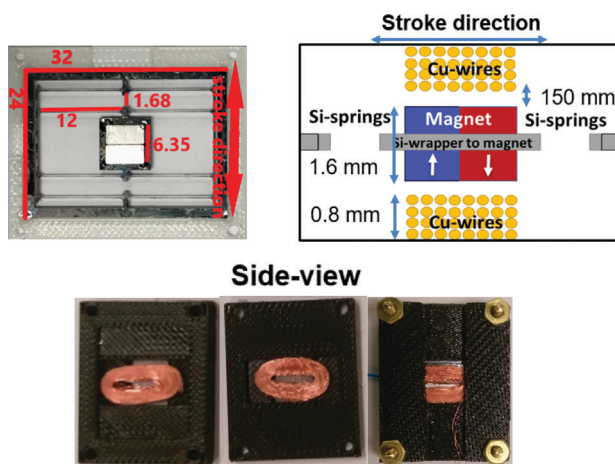
▲ Figure 1: Top: Fabricated harvester dimensions in mm and harvester mechanical concept. Bottom: Disassembled package with the top and bottom coils, and the assembled package..
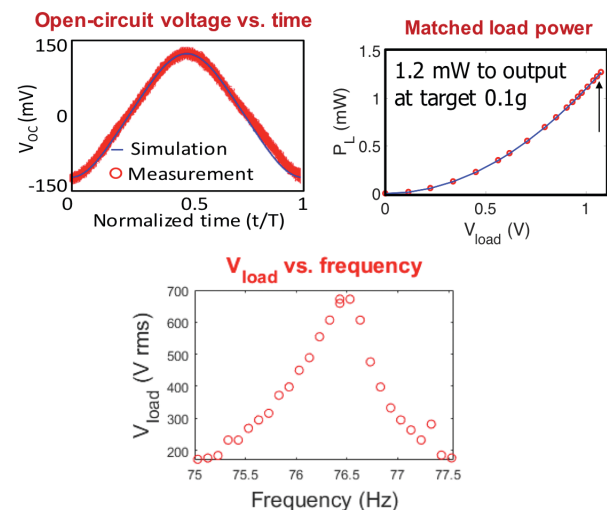
▲ Figure 2: Mechanical harvester's performance plots. The bottom plot shows the device resonance frequency. The narrow curve corresponds to the high Q nature of the device.

FURTHER READING

- U. Radhakrishna, P. Riehl, N. Desai, P. Nadeau, Y. Yang, A. Shin, J. H. Lang, and A. P. Chandrakasan, "A Low-power Integrated Power Converter for an Electromagnetic Vibration Energy Harvester with 150 Mv-AC Cold Startup, Frequency Tuning, and 50 Hz AC-To-DC Conversion," *IEEE Custom Integrated Circuits Conference, (CICC)*, 2018.
- A. Shin, U. Radhakrishna, Q. Zhang, L. Gu, P. Riehl, A. P. Chandrakasan, and J. H. Lang, "A MEMS Magnetic-based Vibration Energy Harvester," *International Conference on Micro and Nanotechnology for Power Generation and Energy Conversion Applications*, (Power MEMS), 2017.

Micro-buckled Beam Based Ultra-low Frequency Vibration Energy Harvester

R. Xu, H. Akay, S.-G. Kim
Sponsorship: MIT-SUTD International Design Center

MEMS energy harvesting has been keenly pursued to provide perpetual power for many wireless applications including distributed sensor networks and upcoming IoT systems. However, scavenging a sufficient amount of power for wireless communication from environmentally available vibrations, typically at low frequency (<70Hz) and low acceleration (0.5g), has neither been successful nor reported at the MEMS scale. Here we present a bi-stable buckled beam MEMS energy harvester which could meet those requirements in terms of low operating frequency, wide bandwidth, and power, all packaged in the size of a coin. This new design does not rely on conventional linear or non-linear resonance of the MEMS structure, but instead operates with large snapping motions of buckled beams at very low frequencies. A fully functional piezoelectric device has been designed, monolithically fabricated, and tested to induce bi-stable buckling of ~200μm. The first batch device generated peak power of 85 nW with 50% half-power bandwidth under 70Hz at 0.5g.

Our bi-stable nonlinear oscillator-based MEMS energy harvester has a clamped-clamped beam structure with a stack of thin-films having 28 pairs of beams 0.4mm wide in a silicon frame of 15mm×12mm. Each beam has approximately 500 interdigitated Au fingers over 0.2 μm thick PZT. A proof mass is located in the middle, connecting the beams to synchronize their out-of-plane motion and minimize undesirable torsion.

Thin-film layers of various stresses have an effective total compression and balanced stress with respect to the neutral axis to achieve bi-stable buckling. The residual stress and the thickness of the thin films are monitored for each deposition step, and progressive feedback control of subsequent deposition is employed to minimize deviation from the design target. The final released device (Figure 1) shows desired bi-stable buckling of about 200μm Figure 2) which is within 5% of the designed value. The dynamic testing with a laser vibrometer validates the design concept that the buckled beam device could have large-amplitude oscillations with low-frequency and low-amplitude inputs (<70Hz and 0.5g).
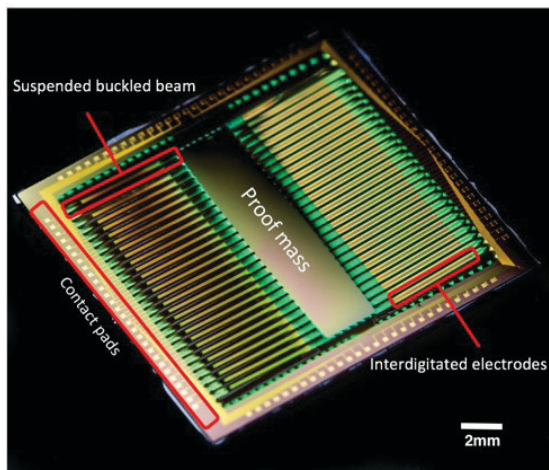
▲ Figure 1: Photo of the released device.
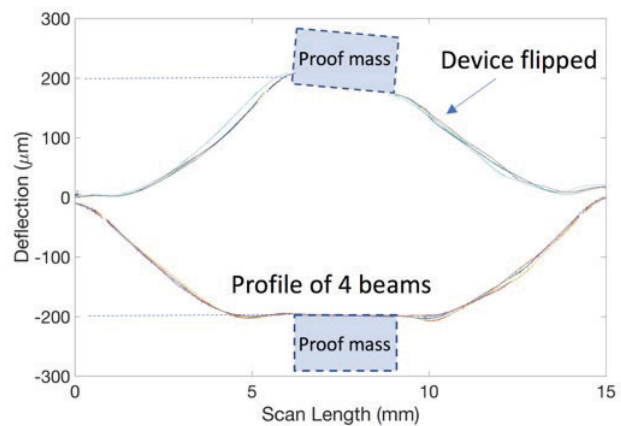
▲ Figure 2. Surface profile scan: Surface profile of four beams showing the buckling on both sides (bi-stable) at around 200 μm.

FURTHER READING

- R. Xu and S.-G. Kim, "Modeling and Experimental Validation of Bi-stable Beam Based Piezoelectric Energy Harvester," *Energy Harvesting and Systems,* vol. 3, no. 4, pp. 313- 321, Nov. 2016.

# RuO$_2$ as Cathode Material of Thin Film Lithium-ion Batteries (LIB)

L. Xu, X. Wang, P. Kumar, D. Perego, A. Weathers, B. Wang, M. Chon, C. V. Thompson
Sponsorship: SMART, MIT Lincoln Laboratory

Technologies for the Internet of Things (IoT) are being developed for a vast number of networking applications. Thin film batteries are important for IoT systems as they are better integrated within an integrated circuit (IC) and can store energy that is harvested by green generators (e.g., solar cells) and provide it to sensors. RuO$_2$ had been found to have a larger specific capacity compared to other cathode materials of lithium ion batteries (LIB), and thus, is a good candidate as a cathode material of thin film LIB. We are currently studying the reaction mechanism of RuO$_2$ and lithium in parallel with the fabrication of full battery devices.

To analyze the mechanism of lithium storage in thin film RuO$_2$, we performed cyclic voltammetry (CV) tests with varying lower limits, as shown in Figure 1. Surprisingly, the lithiation process consists of 3 peaks while the delithiation process consists of 4 peaks. Moreover, the 3rd delithiation peak does not appear in sequential order relative to the other delithiation peaks. To reveal the correspondence between the peaks and specific reactions, *ex situ* cross-sectional TEM, electron diffraction, Raman spectroscopy, and XPS are currently being used.

In addition to characterizing the lithiation of RuO$_2$, we have also built full battery devices that include a lithiated Si anode, a lithium phosphorous oxynitride (LiPON) electrolyte, and RuO$_2$ cathode. Figure 2 shows the cycle performance of the microbattery at a rate of C/10. It could deliver a highly reversible capacity of approximately 150 μAh cm^{-2} μm^{-1} after 100 cycles, which is still 2.5 times higher than commercial CYMBET microbatteries. Ongoing work is focused on improving the cyclability of the RuO$_2$ and silicon anodes through stress engineering, as well as improving the volumetric capacity through process improvements. These initial results suggest a promising route towards IC integratable batteries for on-chip power delivery.
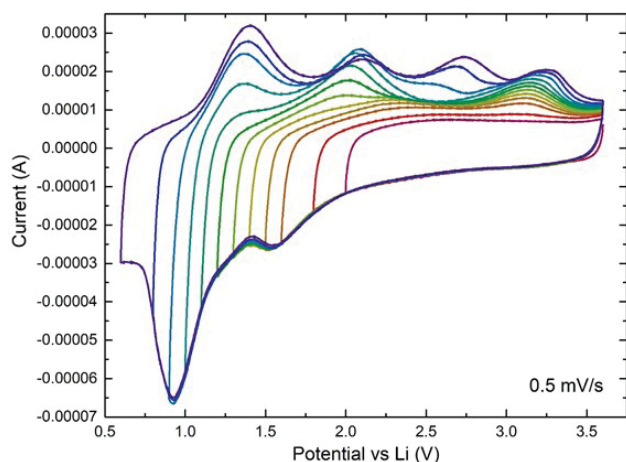
▲ Figure 1: CV scans with varying lower limit of RuO$_2$ thin film. Counter electrode was Li metal, and electrolyte was 1M LiPF$_6$ in 1:1(v:v) EC/DMC.
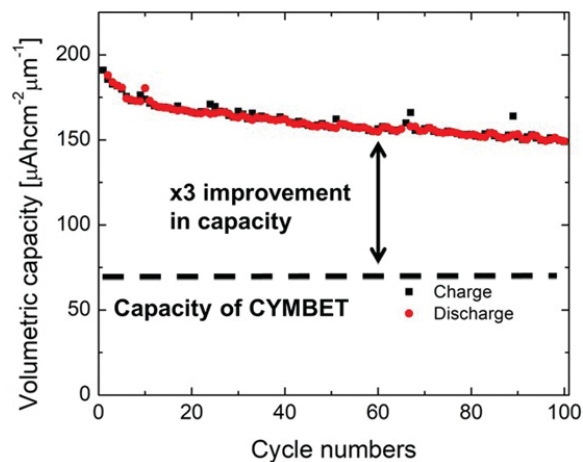
▲ Figure 2: Cycle data of thin film RuO$_2$/LiPON/Li-Si full batteries.
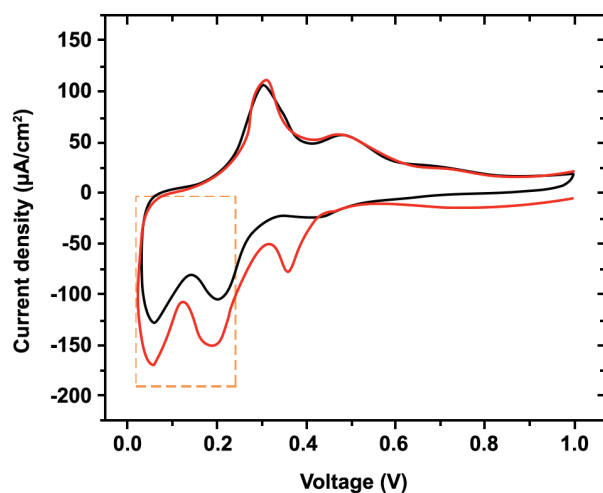
FURTHER READING

- A. Al-Obeidi, D. K. Kramer, S. T. Boles, R. Mönig, and C. V. Thompson, "Mechanical Measurements on Lithium Phosphorous Oxynitride Coated Silicon Thin Film Electrodes for Lithium-ion Batteries during Lithiation and Delithiation," *Appl. Phys. Letts.* vol. 109, pp. 071902, 2016.
- P. Balaya, H. Li, L. Kienle, and J. Maier, "Fully Reversible Homogeneous and Heterogeneous Li Storage in RuO$_2$ with High-capacity," *Advanced Functional Materials,* vol. 13, no. 8, pp. 621–625, 2003.

Kinetic Study of the Reversible Lithiation in Si Thin Film Anodes
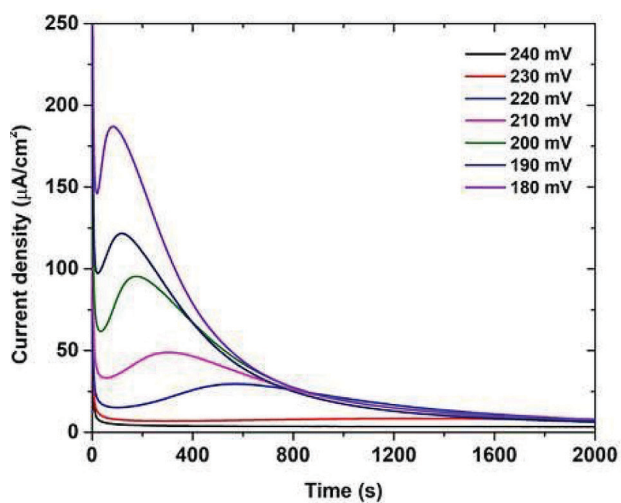
J. Miao, C. V. Thompson
Sponsorship: SMART, Skoltech Center for Electrochemical Energy Storage

Among all the known anode materials for Li-ion batteries, Si is a promising candidate for applications in CMOS-compatible microbatteries. It has extraordinarily high capacities (8375 Ah/cm^3, 3579 Ah/kg), which is a result of the unique alloying mechanism during lithiation that involves bond breakage and a series of formation of new short-range structures. The reversible lithiation of Si anodes (Figure 1, highlighted) has not been extensively studied, and there have also been debates over whether it is a diffusion process or a phase-transition process. Here we adopt the potentiostatic technique to study the reversible phase transitions that occur in the second and subsequent lithiation cycles.

It was found that there is always a peak in the current vs. time curve under desirable potentiostatic test conditions in the reversible lithiation regime (Figure 2). The existence of the peak suggests there is phase transition in the reversible lithiation, rather than pure diffusion where current should decrease monotonically with time. The time at which the peak occurs (t_{peak}) increases with the applied potential, which indicates slower kinetics for the phase transition. Kinetic parameters could be extrapolated from the current vs. time curves upon modeling and fitting.

▲ Figure 1: CV (cyclic voltammogram) curves in the first and second cycles of a LiPON-coated Si thin film sample. The highlighted voltage regime indicates the reversible lithiation regime. The scan rate is 40 μV/s.

▲ Figure 2: Current vs. time curves at different voltages (180, 190, 200, 210, 220, 230, 240 mV, respectively) after a potentiostatic hold at 270 mV for 4.5 hours in a LiPON-coated Si thin film sample (180 nm thick).

FURTHER READING

- J. Miao and C. V. Thompson, "Kinetic Study of the Initial Lithiation of Amorphous Silicon Thin Film Anodes," *J. of the Electrochemical Society,* vol. 165, no. 3, pp. A650-A656, 2018.

Modeling Discharge Pathways in Li-O$_2$ Batteries to Optimize Capacity

T. Batcho, Y. Shao-Horn, C. V. Thompson

Li-O$_2$ batteries offer the possibility of storing twice the gravimetric energy density of Li-ion batteries. Li-O$_2$ batteries operate by reacting oxygen with lithium ions in a non-aqueous solvent to form Li$_2$O$_2$ on a conductive cathode material. However, Li$_2$O$_2$ has poor electronic conductivity and passivates the electrode area. Achieving high capacity requires careful attention to Li-O$_2$ discharge mechanisms in order to optimize cathode void space filling by Li$_2$O$_2$.

Li-O$_2$ discharge occurs by two competing mechanistic pathways which are responsible for two possible morphologies of Li$_2$O$_2$ discharge product. The surface pathway involves two consecutive electron transfers to form a ~10 nm thin film of Li$_2$O$_2$. The solvent pathway involves the solvation of the reaction intermediate Li$^+$-O$_2^-$, which then reacts in solution to form ~100 nm in diameter toroids of Li$_2$O$_2$. Since toroids allow for greater volumes of Li$_2$O$_2$ to form with less electrode area coverage, toroids are preferable to maximize capacity. However, the exact dependence of each pathway on different discharge conditions and solvent properties to promote toroid formation is not fully understood.

Rotating ring-disk electrode (RRDE) experiments were performed to understand these pathway trends. A rotating rod creates convection currents that sweep reactants to the central disk electrode (Figure 1). Li$_2$O$_2$ film and soluble Li$^+$-O$_2^-$ are formed at the disk. Soluble Li$^+$-O$_2^-$ is swept to the ring electrode and oxidized, providing a measure of the relative size of the solvent pathway. By comparing ring and disk currents, the separate contribution of each discharge pathway can be determined.

We then developed a model based on nucleation and growth of the Li$_2$O$_2$ film to explain potentiostatic discharge curves collected from RRDE experiments under different discharge conditions, such as varying solvent water content (Figure 2). The model demonstrates that high Li$^+$-O$_2^-$ solvent solubility inhibits the surface pathway and that this effect is primarily responsible for toroid promotion.
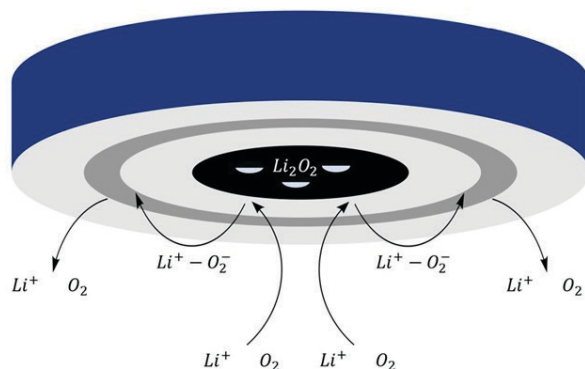
▲ Figure 1: Schematic of RRDE setup. Disk electrode in black; ring electrode in dark gray. Li$_2$O$_2$ film deposits on the disk. Toroid precursor Li$^+$-O$_2^-$ oxidizes at the ring.
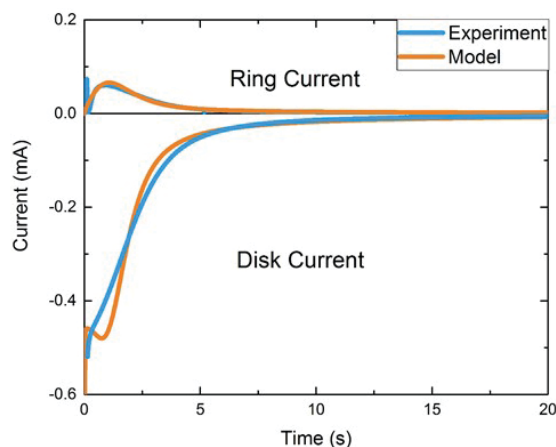
▲ Figure 2: Model fit (orange) of experimental disk and ring currents (blue) collected at 2.4 V vs. Li$^+$/Li at 1600 rpm in 0.1M LiClO$_4$ DMSO.

FURTHER READING

- R. R. Mitchel, B. M. Gallant, Y. Shao-Horn, and C. V. Thompson, "Mechanisms of Morphological Evolution of Li$_2$O$_2$ Particles during Electrochemical Growth," *J. of Physical Chemistry Letts.*, vol. 4, no. 7, pp. 1060, Mar. 2013.
- D. G. Kwabi, M. Tulodziecki, N. Pour, D. M. Iitkis, C. V. Thompson, and Y. Shao-Horn, "Controlling Solution-mediated Reaction Mechanisms of Oxygen Reduction using Potential and Solvent for Aprotic Lithium-oxygen Batteries," *J. of Physical Chemistry Letts.*, vol. 7, no. 7, pp. 1204–1212, Mar. 2016.

Multi-cell Thermogalvanic Systems for Harvesting Energy from Cyclic Temperature Changes

L. Xu, P. A. Linford, B. Huang, C. V. Thompson, Y. Shao-Horn
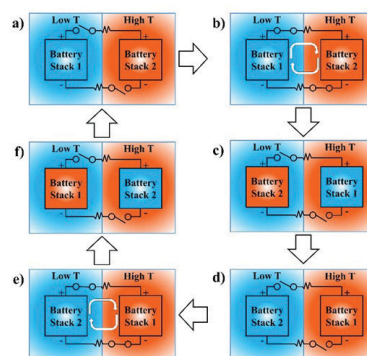Sponsorship: HKUST-MIT Research Alliance Consortium

Technologies for the Internet of Things (IoT) are being developed. An IoT network consists of large quantities of networked sensors that are often in remote or difficult to access locations, which drives the need for self-powered systems. Here, we come up with two types of multi-cell thermogalvanic systems that generate electrical power through temperature cycles.

The dual-temperature, dual-stack, self-powered electrochemical system is depicted in Figure 1. This dual-temperature system uses two identical electrochemical stacks, which can be a single battery or multiple batteries connected in series; however, each electrochemical stack is held at a different temperature. On the other hand, a single-temperature system works similarly, with the electrochemical stacks having similar operating potentials but oppositely signed temperature coefficients. Its operation is illustrated in Figure 2. Both systems can harvest energy from temperature cycles.

We have tested both dual-temperature systems and single-temperature systems with different cathode/anode materials, load resistances, and frequencies of temperature cycles. The largest energy conversion efficiency was obtained from the dual-temperature experiment with two homemade $LiCoO_2$/Li coin cells in which the cathodes with composition $Li_{0.85}CoO_2$ were cycled between 20 °C and 50 °C. The loads were two 100Ω resistors. The current is shown in Figure 3, and the efficiency was calculated to be 0.22%. This value is comparable to the efficiency obtained using charging-free thermally regenerative electrochemical cycles (TRECs), thermocapacitive cycles and ionic thermoelectric supercapacitors, but with more flexibility of material selection. In the meantime, we have also tested two single-temperature systems with four LiV_2O_5/Li-Al and three $LiCoO_2$/Li cells, and one $LiMnO_2$/Li-Al and one LiV_2O_5/Li-Al cell, respectively. Although the efficiency and power were still limited, they confirmed the feasibility of this concept. These systems can be further optimized by using materials with higher temperature coefficients and decreasing internal resistance at the same time.

▲ Figure 1: Schematic of dual-temperature system.
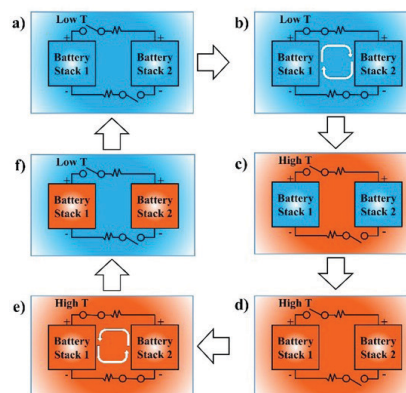
▲ Figure 2: Schematic of single-temperature system.

▲ Figure 3: Results from the dual-temperature test with two 100Ω resistors and two homemade $LiCoO_2$/Li cells using LP57 electrolyte and Celgard 2500 separators.
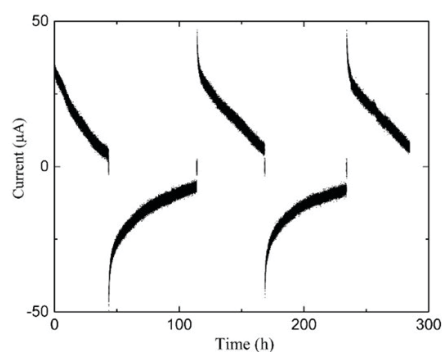
FURTHER READING

- A. Härtel, M. Janssen, D. Weingarth, V. Presser, and R. van Roji, "Heat-to-Current Conversion of Low-grade Heat from a Thermocapacitive Cycle by Supercapacitors," *Energy Environ. Sci.*, vol. 8, pp. 2396–2401, 2015.
- Y. Yang, S. W. Lee, H. Ghasemi, J. Loomis, X. Li, D. Kraemer, G. Zheng, Y. Cui, and G. Chen, "Charging-free Electrochemical System for Harvesting Low-grade Thermal Energy," *PNAS*, vol. 111 no. 48, pp. 17011–17016, 2014.